Published on 04 February 2016. Downloaded by CHINA PHARMACEUTICAL UNIVERSITY LIBRARY on 20/12/2016 09:52:56.

NJC

PAPER

View Article Online
View Journal | View Issue

Cite this: *New J. Chem.*, 2016, **40**, 4480

Superparamagnetic Fe_3O_4 nanoparticles: synthesis by a solvothermal process and functionalization for a magnetic targeted curcumin delivery system

Man Qi,[a] Kai Zhang,[a] Siqiao Li,[a] Jianrong Wu,[a] Chuong Pham-Huy,[b] Xintong Diao,[a] Deli Xiao*[a] and Hua He*[ac]

Received (in Montpellier, France) 11th September 2015, Accepted 4th February 2016

DOI: 10.1039/c5nj02441b

www.rsc.org/njc

Tailoring surface characteristics is necessary for the biomedical application of superparamagnetic Fe_3O_4 nanoparticles. This study developed an approach for the synthesis of Fe_3O_4 nanoparticles with different functional groups grasped on the surface and the influence of different functionalization on the behavior of drug loading and release was also assessed. Monodisperse Fe_3O_4 nanoparticles were first prepared through a novel and simplified solvothermal process. The resulting oleylamine coated nanoparticles (about 4.3 nm in diameter) were carboxylated by *meso*-2,3-dimercaptosuccinic acid (DMSA) ligand-exchange reactions and further development of amino-functionalized nanoparticles (Fe_3O_4@DMSA–NH_2 NPs) was achieved by chemical reaction with a short chain molecule ethanediamine *via* 1-ethyl-3-(3-dimethylaminopropyl)-carbodiimide hydrochloride activation of the carboxylic acids on the surface of DMSA-coated Fe_3O_4 NPs. The two types of functionalized magnetic nanoparticles with –COOH and/or $-NH_2$ fabricating their hydrophilicity were characterized and designed as drug carriers to load a natural antitumor drug, curcumin (CUR), which is water-insoluble and instable. The loading process could be described by the Langmuir adsorption isothermal model and pseudo-second-order kinetic model for both functionalized Fe_3O_4 NPs and a stronger drug-loading ability was observed from the Fe_3O_4@DMSA–NH_2 NPs. Furthermore, it's worth noting that all the particles showed a relatively pH-sensitive drug release and the Fe_3O_4@DMSA–NH_2 NPs showed a prolonged drug release, which makes them suitable for use as a scaffold for the design of a pH-sensitive based controlled release carrier. Due to those properties, the functionalized nanoparticles have great promise to be developed as a magnetic targeted drug delivery system for hydrophobic drugs.

Introduction

Nowadays, cancer has become the major factor which threatens the health of people and the means of nonsurgical therapy mainly include radiotherapy and chemotherapy. Many of the chemotherapeutic drugs lack selectivity for tumors and often elicit toxicity to normal cells even under optimal conditions. Given this, precisely targeting drugs to diseased cells has become increasingly important in tumor treatment.[1] The last decades has witnessed various targeted drug delivery strategies explored for drug targeting, among which, magnetic targeted drug delivery systems (MTDDS) have been found to be excellent approaches due to their non-specificity for various solid tumors and easy control with an external magnetic field.[2–4]

Over the years, there were numerous nanoparticulate preparations applied to magnetic targeted drug delivery and applications including cellular therapy, hyperthermia, magnetic resonance imaging (MRI) and tissue repair. Superparamagnetic Fe_3O_4 nanoparticles (SPIONs) have characteristics which give them potential, *e.g.*, easy-prepared, small size, low-toxicity and unique magnetism.[5,6] Furthermore, especially size factors promoting the accumulation of a drug at tumor sites through the enhanced permeability and retention effect (EPR) have given rise to their widespread application in magnetic targeting drug delivery, and they have even been approved to be used as a contrast agent for tumor imaging by the U.S. Food and Drug Administration (FDA).[7] Recent animal clinical trials have further confirmed that SPIONs, a functional material, have a great future in the development of targeting technology.[8–10]

In past decades, there were various preparations based on Fe_3O_4 nanoparticles applied to nanomedicine. However, just as a scaffold for developing MTDDS, raw Fe_3O_4 nanoparticles have

---

[a] *Department of Analytical Chemistry, School of Sciences, China Pharmaceutical University, Nanjing 210009, Jiangsu, China. E-mail: jcb315@163.com, dochehua@163.com, xiao49562000@163.com; Fax: +86 025 83271505; Tel: +86 025 83271505*

[b] *Faculty of Pharmacy, University of Paris V, Paris, 75006, France*

[c] *Key Laboratory of Drug Quality Control and Pharmacovigilance, Ministry of Education, China Pharmaceutical University, Nanjing 210009, China*

This journal is © The Royal Society of Chemistry and the Centre National de la Recherche Scientifique 2016

Published on 04 February 2016. Downloaded by CHINA PHARMACEUTICAL UNIVERSITY LIBRARY on 20/12/2016 09:52:56.

defects such as poor water dispersibility, bad chemical stability and lack of functional groups for effectively conjugating biomolecules and pharmaceutical compounds, which lead to a low load capacity. Given this, how to prepare SPIONs with small size, narrow size distribution, high saturation magnetization, good crystallinity and further functionalization for different applications is of essential importance.[11,12]

Currently, there are several ways to prepare magnetic nanoparticles (MNPs), in which solvothermal decomposition and a co-precipitation method are typical representatives of a homogeneous reaction system. Compared with a co-precipitation method, the solvothermal decomposition process operated at high-temperature and with high-pressure surroundings possesses the advantages to construct nanocomposites with satisfactory properties as described above, sparking tremendous popularity among materials research areas.[13–15] This mainly results from these reasons: (1) solvothermal decomposition performed at high temperature allows the control of the nucleation and growth of nanocrystals; (2) adoption of the organic phase can sequester the participation of water which could easily coordinate with iron ions.

In addition to the preparation of initial nanoparticles, further surface functionalization is also a necessary prerequisite for constructing MNP based drug delivery.[9,16] Nanoparticles carrying such organic functional groups as –COOH, $-NH_2$, –OH, *etc.* can achieve an effective connection to drug molecules through chemical bonds, hydrogen bonds or physical interactions and achieve their controllable release as well, which depends on the pH and temperature variation in different tissues and cellular compartments [the tumor has a lower pH (∼5–6) than normal tissues pH (∼7.4)].[17–19] For instance, Hua's group developed a nontoxic drug carrier based on MNPs (8 nm in diameter) modified with a water-soluble polyaniline derivative, poly[aniline-*co*-sodium *N*-(1-one-butyric acid)aniline] (SPAnNa). The fabricated SPAnH/MNPs formation containing carboxyl groups can covalently bind the hydrophobic drug paclitaxel and greatly improve its adsorption amount and water solubility.[20] In the study of Shun Yang *et al.*, a multifunctional pH-sensitive nanocomposite for targeted drug delivery and MRI was prepared *via* a self-assembly process. The formation consists of hollow mesoporous silica nanoparticles (HMS) modified by hydrocarbon octadecyltrimethoxysilane (C18) as a core, a pH-sensitive amphiphilic polymer (HAMAFA-*b*-DBAM) as a shell and SPIONs fixed between the two segments mentioned above. The model drugs were loaded in the hollow core of the HMS and the nanocomposites could be easily tracked by MRI due to the magnetism of the encapsulated SPIONs. In addition, the amphiphilic polymer conjugated with folic acid (FA) endowed the carrier with pH-sensitive drug release and allowed it to biologically target the folic acid receptor (FR) of over-expressed tumor cells.[21]

Curcumin (CUR), a natural polyphenol component extracted from the underground rhizome of tumeric, has gained considerable attention recently because of its multiple pharmacological activities, including anti-inflammatory, antioxidant, anti-bacterial, and antiviral activities and its especially wide spectrum of actions against tumors.[11,22] Favourably, no obvious toxicity or side effects were found when used for a long period.[22] Recent research implies that curcumin is also an effective multidrug resistance (MDR) reversal agent. Curcumin has been considered as one of the ideal anti-cancer chemicals. However, its widespread application in clinic tumor therapy is greatly hindered by its water-insolubility, instability and thus low bioavailability. In spite of the disadvantages, inspired by its specific biological activity and simple molecular structure, curcumin is still considered as an excellent lead compound for structure modification and selection of anti-tumor drugs.[23] In recent years, aimed at improving hydrophilicity and anti-tumor effect, research on building hydrophilic CUR preparations has proved to be an effective strategy to tackle the problem and have attracted great interest from researchers. To date, although many nanotechnology investigations focused on either improving hydrophilicity or bioavailability of CUR, achieving the micromolar concentrations at which CUR exhibits anticancer effects at the tumor site in humans is highly challenging and has not yet been accomplished.[22]

In this study, superparamagnetic Fe_3O_4 nanoparticles (∼4.3 nm in diameter) with narrow size distribution, chemical stability and good magnetic response were first prepared *via* a simplified thermal decomposition method. Then the resulting oleylamine coated Fe_3O_4 nanoparticles were functionalized to construct targeted drug delivery systems for loading the natural anti-cancer drug CUR, and the loading and release behavior was systematically investigated. Although sound scientific literature is available on drug loading on functionalized MNPs, systemic studies of the effects of different functional groups on the loading and release of CUR are rarely reported. As is indicated in the results, the as-fabricated functionalized Fe_3O_4 nanoparticles obtained from a ligand exchange reaction and subsequent amination can significantly improve the loading behavior of CUR. Furthermore, the hydrophilic groups on the surface of the magnetic nanoparticles endow the carrier with good water solubility and stability. In summary, the as-developed MNP-mediated drug delivery nanoformulations with high loading capacity and hydrophilicity are expected to be used as a scaffold for the design of a CUR carrier and enable the effective concentration at tumor sites. Our study will enrich the basis theory on surface-engineered MNPs and provide a reference for the design of MTDDS for hydrophobic drugs.[24]

Experimental

Materials

Iron(III) acetylacetonate [$Fe(acac)_3$], oleylamine, benzyl ether and other chemical reagents were purchased from Sinopharm Chemical Reagent Co. Ltd. *meso*-2,3-Dimercaptosuccinic acid (DMSA), ethane diamine, 1-ethyl-3-(3-dimethylaminopropyl)-carbodiimide hydrochloride (EDC·HCl) were obtained from Aldrich Chemical Co. All reagents mentioned above were of analytical reagent grade and used as received. The drug curcumin (CUR) was supplied by Sigma-Aldrich and its chemical structure is shown in Fig. 1a.

Synthesis of superparamagnetic iron oxide nanoparticles

The SPIONs were prepared using a very simplified solvothermal route.[25] In a typical synthesis, 22.5 mL of oleylamine and 7.5 mL

Published on 04 February 2016. Downloaded by CHINA PHARMACEUTICAL UNIVERSITY LIBRARY on 20/12/2016 09:52:56.

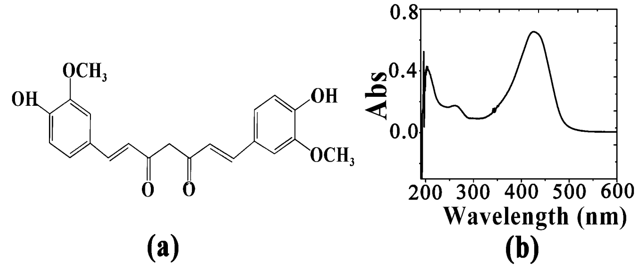

Fig. 1 (a) The structure of CUR and (b) the UV-Vis spectra of CUR 75% ethanol water solution at a concentration of 10 μg mL^{-1}.

of benzyl ether were mixed in a warm water bath. Afterwards, $Fe(acac)_3$ (3 mmol) was dissolved into the solution with ultrasonication for 30 minutes. The light brown dispersion obtained was transferred into a Teflon-lined stainless-steel autoclave, followed by flushing with nitrogen to eliminate trace oxygen and moisture, and then the mixture was heated to 200 °C and aged at this temperature for 2 hours. After the reaction, the solution was allowed to cool down to room temperature. The product was extracted upon the addition of ethanol, followed by a centrifugation recovery process several times to remove residual reagents. The final black materials were dried in a vacuum at 30 °C overnight and designated as Fe_3O_4@Oley NPs.

Carboxylation of iron oxide nanoparticles

The as-prepared Fe_3O_4@Oley NPs were only oil-soluble. The carboxylation of the Fe_3O_4 NPs with DMSA was carried out by a direct route, during which hydrophobic Fe_3O_4 NPs were successfully transformed to be hydrophilic magnetite nanoparticles (Fe_3O_4@DMSA NPs).[26,27] 300 mg of dried Fe_3O_4@Oley NPs dispersed into 20 mL of toluene were added into a container containing a solution of DMSA (300 mg, 1.07 mmol) in 20 mL of DMSO. Then the mixture was sonicated for 1.5 h, followed by shaking with a rotary shaker at 185 rpm for 36 h at room temperature. Afterwards, the supernatant was discarded and the resulting functionalized nanoparticles were mixed with ethanol and water, followed by centrifugation to eliminate free oleylamine molecules. The washing procedure was repeated several times before redispersing the carboxylated nanoparticles into water. Finally, the pH of the aqueous suspension was adjusted to 10 with NaOH solution to deprotonate the carboxylic groups and thiol groups of the DMSA. Then the pH was tuned to 7 with HNO_3 solution in order to achieve a stable dispersion of Fe_3O_4@DMSA NPs. The surface carboxyl groups on the Fe_3O_4@DMSA NPs were determined with a titration method and the content was calculated to be 1.63×10^{-3}–1.65×10^{-3} mol g^{-1}.[28,29]

Amination of iron oxide nanoparticles

The amination of iron oxide nanoparticles was achieved *via* an ethyl-3-(3-dimethylaminopropyl)-carbodiimide hydrochloride (EDC·HCl)-mediated amidation reaction with a small molecule, ethane diamine. The coating process was carried out in an ice water bath under ultrasonic waves. An aqueous suspension containing 150 mg Fe_3O_4@DMSA NPs was mixed with ethane diamine (8 mL). The resulting solution was mixed with EDC·HCl (30.0 mg), which was divided into six aliquots, one of which was added every 120 min, and the sixth 16 h after the previous addition. The molar ratio of COOH/NH_2/EDC·HCl was valued as 1 : 1.6 : 1.2. Afterwards, the pH was tuned to 6 with a HCl solution and then the mixture was sonicated for 6 h, followed by circularly shaking for 48 h at room temperature. Then the formed nanoparticles (denoted as Fe_3O_4@DMSA–NH_2 NPs) were collected using an external magnet and washed several times with ethanol and water, and finally dispersed into water.

The whole functionalization process is illustrated in Fig. 2.

Characterization

The morphology and size of the products were examined using a FEI Tecnai G2 F20 transmission electron microscope (TEM). The hydrodynamic radius and zeta-potential measurements of the particles were performed with dynamic light scattering (DLS) equipment (Brookhaven, USA). Phase identification was carried out with an X'TRA X-ray diffractometer with Cu Kα irradiation at $\gamma = 0.1541$ nm. The measurements were conducted in the 2θ range of 10–70° with a scanning velocity of 2° min^{-1}. The surface groups on nanocomposites were measured with an 8400 s FTIR spectrometer (Shimadzu Corporation, Japan) with KBr pellets.[30] Elemental analysis was carried out using a Vario EL III Elemental analyser. The magnetic properties of the obtained samples were investigated using a LDJ9600-1 vibrating sample magnetometer (VSM) operating at room temperature with applied fields of up to 10 kOe. The ultraviolet-visible (UV-Vis) spectrum of curcumin was recorded with a Shimadzu UV-1800 spectrophotometer (Japan) equipped with 1.0 cm quartz cells.

The investigation of the stability of CUR

To determine the detecting wavelength, a 75% ethanol water solution containing curcumin at a concentration of 5 μg mL^{-1} was prepared and scanned using a UV-Vis spectrophotometer at a range of 200–600 nm. The characteristic absorption spectrum is shown in Fig. 1b. The maximum wavelength 426 nm was selected as the detection wavelength.

Because it is easily affected by complex environmental factors, such as pH, light and temperature, the stability of CUR was investigated for the purpose of developing ideal experiment conditions under which CUR was stable. To investigate the influence of pH on the stability of CUR, a series of buffer solutions in an equal concentration at different pH values (3.0 to 10.0) were prepared and kept in the dark at room temperature. A certain volume of the solution was withdrawn at predetermined intervals and the absorbance was measured at 426 nm using a UV-Vis spectrometer. With a 75% ethanol–water mixture used as a solvent, a study of the effect of light on the UV-Vis absorbance of CUR was performed under dark and lighting conditions, respectively. In addition, different temperature (4 °C, 25 °C, 37 °C, 60 °C) treatments were carried out to evaluate the thermal stability of CUR. The estimation of the effect of light and temperature on CUR stability using UV-Vis spectrophotometry was carried out in a similar manner as the study of pH.

The results of the investigation of the stability of CUR are shown in Fig. 3. Fig. 3a represents the influence of pH on the

Published on 04 February 2016. Downloaded by CHINA PHARMACEUTICAL UNIVERSITY LIBRARY on 20/12/2016 09:52:56.

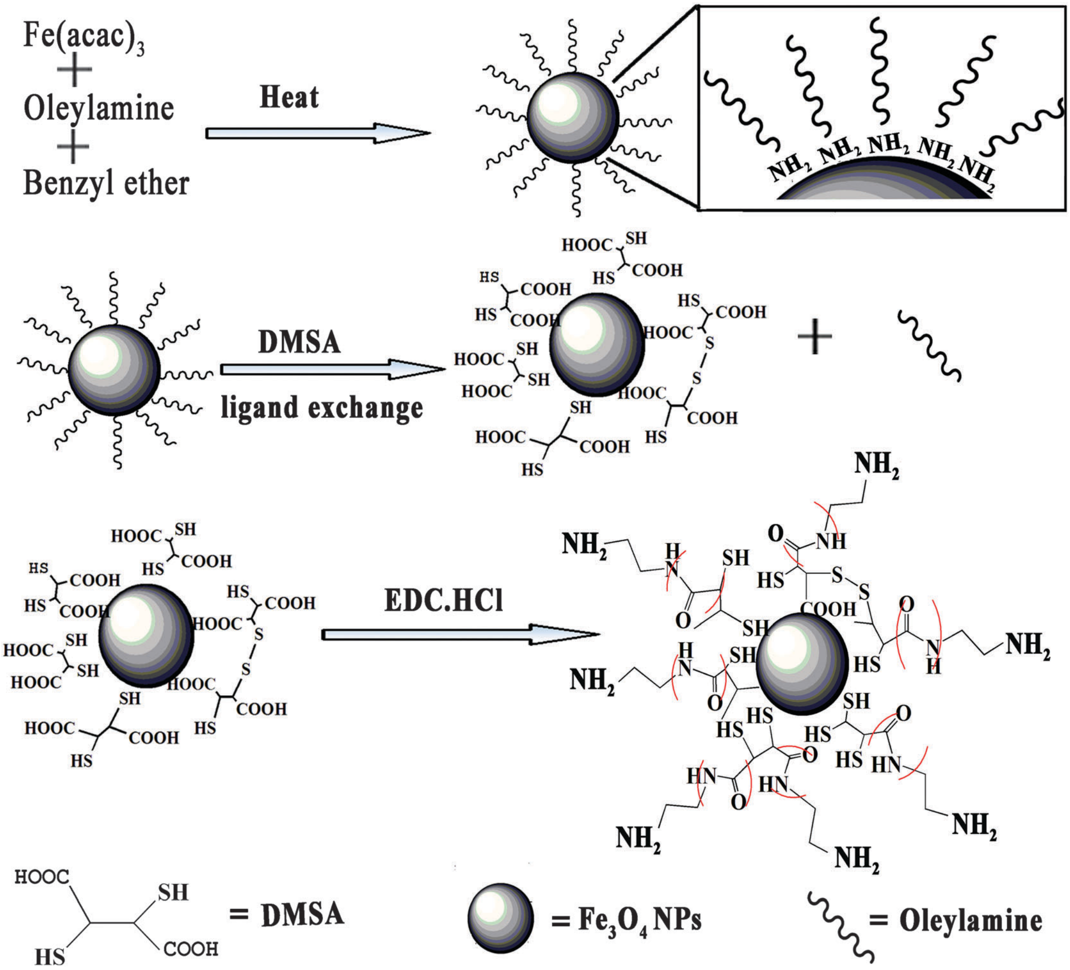

Fig. 2 Schematic illustration of the functionalization process of SPIONs.

stability of CUR. It was observed that the changes in the UV-Vis absorbance were pH-dependent and the decomposition occurred quickly under neutral and alkaline conditions.[31] Fig. 3b shows an easy degradation of CUR because of light. The results of the stability testing performed under various temperatures are depicted in Fig. 3c. The absorbance values of the CUR solutions deposited at temperatures of 4 °C, 25 °C and 37 °C present relatively small changes within the error range allowed, while the sample incubated at 60 °C has a much bigger variation, indicating the thermal instability of CUR at high temperatures. All the investigations on the stability of CUR described above suggest that the experiments on CUR should be carried out at low temperature, low pH and dark conditions.

Adsorption experiments

CUR standard solutions at different concentrations of 1–9 μg mL^{-1} were prepared and the absorbance was measured using a UV-Vis spectrometer to establish the homologous standard curve, from which the concentration of the CUR solutions could be calculated. The background effect of the particle solution was deducted during the measurement.

To evaluate the adsorption kinetics of curcumin onto functionalized particles, 50 mL of designed curcumin 75% ethanol water solutions at a concentration of 200 μg mL^{-1} containing 40 mg of Fe_3O_4@Oley NPs, Fe_3O_4@DMSA NPs or Fe_3O_4@DMSA–NH_2 NPs were prepared respectively. Samples were withdrawn at different time intervals until the adsorption reached equilibrium.

To evaluate the adsorption capacity of different particles, static equilibrium adsorption experiments were conducted in 5 mL screw-capped glass centrifuge tubes at 25 °C. Each tube containing 5.00 mg Fe_3O_4@Oley, Fe_3O_4@DMSA NPs, or Fe_3O_4@DMSA–NH_2 NPs, respectively were filled with 4 mL of the pre-prepared 75% (v/v) ethanol water containing CUR at different concentrations. All tubes were sealed and shaken persistently using a rotary shaker at 185 rpm for 6 h.

All adsorption experiment batches were performed in the dark at ambient temperature (25 ± 2 °C) and the pH of all the adsorption systems was kept at 5.4. Samples were magnetically separated from the reaction mixture and the clear supernatant from each sample was taken to measure the absorbance at λ = 426 nm with a UV-Vis spectrophotometer. The data measured were used to estimate the loading quantity of CUR according to the following expression:

$$q_t = \frac{(C_0 - C_t)V}{m} \quad (1)$$

Published on 04 February 2016. Downloaded by CHINA PHARMACEUTICAL UNIVERSITY LIBRARY on 20/12/2016 09:52:56.

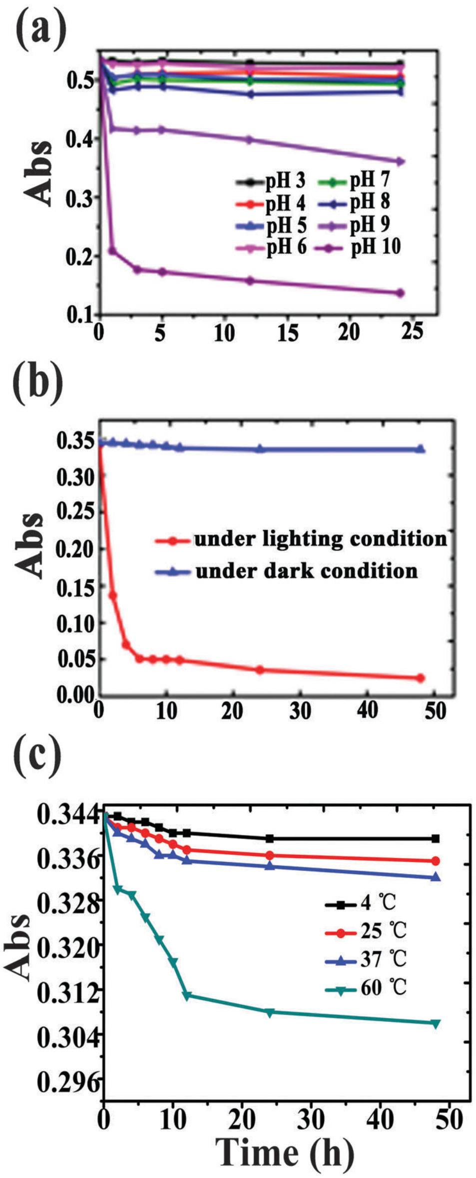

Fig. 3 The results of the influence of (a) pH, (b) light and (c) temperature on the stability of CUR.

where q_t is the amount of CUR loading on the nanoparticles (mg g^{-1}); C_0 and C_t (mg g^{-1}) respectively represent the CUR concentrations in the supernatant initially and at time t (min); V is the total volume (L) of the solution and m is the mass of the particles used in the adsorption experiments.

In vitro release of CUR

For the drug release study, the suspensions of CUR loaded Fe_3O_4@Oley, Fe_3O_4@DMSA NPs and Fe_3O_4@DMSA–NH_2 NPs (20 mg) were allowed to stand at 37 °C in two phosphate-buffered saline (PBS) solutions containing 0.1% weight/volume SDS (Sigma-Aldrich) at pH 7.40 and 5.38, respectively. Then the mixture was shaken with a rotary shaker at 185 rpm persistently. At predetermined intervals, 3 mL of the release medium was withdrawn and centrifuged at 13 000 rpm for 2 minutes and the supernatant was stored at 4 °C in the dark. Then equal volumes of the fresh medium were replaced in the tube to redisperse the particles. The collected supernatants were measured by spectrophotometry at 426 nm as described earlier.

Results and discussion

Synthesis and characterization

Monodisperse SPIONs were first fabricated by a direct and simple solvothermal method based on the decomposition of $Fe(acac)_3$ in a hot solvent solution. According to the reports published, among all the synthetic procedures developed so far, thermal decomposition of $Fe(acac)_3$ in a hot organic solvent in the presence of a reducing reagent and surfactant was first demonstrated to be an ideal way to synthesize monodisperse Fe_3O_4 NPs.[15,32–34] In a typical procedure, SPIONs are prepared in a mixture of oleylamine and oleic acid. In this paper, the SPIONs were fabricated through a simplified route in which oleylamine was used as both a reducing reagent and a surfactant which was inexpensive and could create much stronger reductive circumstances than the alkanediols used in previous reports.[35] The excess amount of oleylamine is the key to the thermal decomposition of $Fe(acac)_3$ and could facilitate the reaction at a lower temperature. It is noted that the size and the shape of the SPIONs could be tuned by controlling the heating conditions and the ratio of oleylamine to benzyl ether. The detailed interpretations were clarified as in reports by Xu *et al.*[15]

The morphology and size of different functionalized SPIONs including Fe_3O_4@Oley, Fe_3O_4@DMSA, Fe_3O_4@DMSA–NH_2 were examined using TEM (Fig. 4) and the corresponding size distributions are presented in the bottom-right corner of each photo. The particle sizes were arithmetically averaged directly to build size distributions by counting ∼100 particles for each sample. Fig. 4a is the TEM image of the Fe_3O_4@Oley NPs. It was observed that the average size of the particles was ∼4.3 nm with a narrow distribution of 3.9–6.4 nm. The shape was uniform and nearly spherical. This was attributed to the interaction of oleylamine with $Fe(acac)_3$ during the nucleation and growth phase which may aid the crystal growth to become spherical-shaped which would have the lowest surface free energy and colloidal stability in organic solvents. In Fig. 4b, the mean diameter of the Fe_3O_4@DMSA NPs, fabricated using a ligand-exchange reaction, determined from the TEM image was about 9.5 nm with a much larger size distribution than that of the Fe_3O_4@Oley NPs. Besides, the shape of the particles in the visual field was free-form.

This might attributed to the fact that the particles became instable and aggregated during the intermediate process in which the oleylamine was replaced and DMSA did not cover the particles effectively yet.[14] Fig. 4c is the TEM image of the Fe_3O_4@DMSA–NH_2 NPs. There was no significant difference in shape and size distribution from that of the Fe_3O_4@DMSA NPs due to the amidization reaction occurring at the end of the DMSA molecules.

Hydrodynamic size (D_h) is a greatly important assessment of particles for biomedical applications. Only nanoparticles with appropriate D_h could avoid uptake by the reticuloendothelial

Published on 04 February 2016. Downloaded by CHINA PHARMACEUTICAL UNIVERSITY LIBRARY on 20/12/2016 09:52:56.

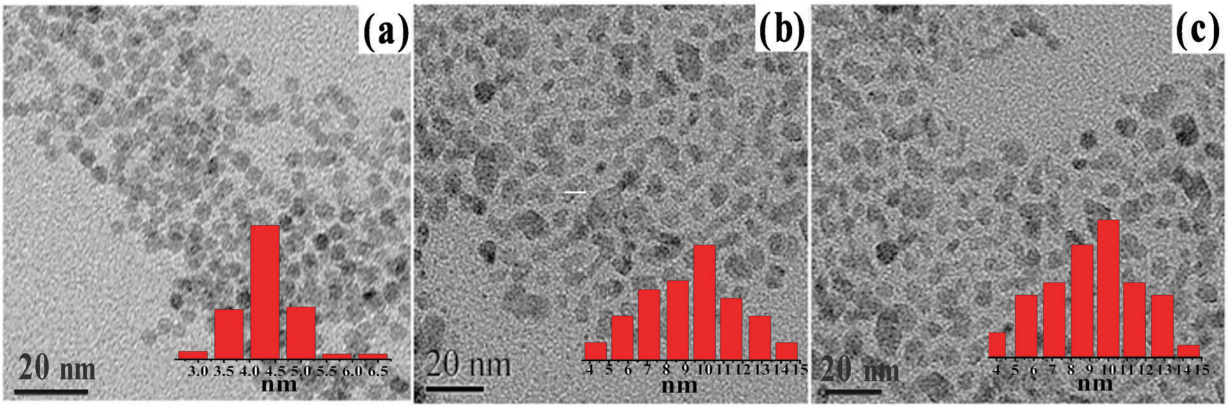

Fig. 4 TEM images and size distributions of (a) Fe_3O_4@Oley, (b) Fe_3O_4@DMSA and (c) Fe_3O_4@DMSA–NH_2 NPs.

system (RES) and reach the diseased tissues. The D_h of different Fe_3O_4 nanoparticles was measured using DLS. As shown in Fig. 5A, the sizes of the Fe_3O_4@Oley, Fe_3O_4@DMSA and Fe_3O_4@DMSA–NH_2 NPs were ~7.3 nm, ~19.5 nm and ~20.8 nm, respectively. The D_h of all nanoparticles were larger than the TEM sizes. This kind of increase in size may result from the fact that the DLS gives the mean size of the magnetite core surrounded by the solvation layers, whereas the TEM diameter is based on the samples alone in a dry state.[36,37] Because of the exchange of ligands, the D_h and polydispersity index (PDI) of the two types of functionalized Fe_3O_4 nanoparticles were bigger than that of the initial nanoparticles (PDI = 0.16 ± 0.06) which was consistent with the TEM results. The PDIs of the two types of functionalized particles were low (PDI = 0.26 ± 0.08 for Fe_3O_4@DMSA NPs and PDI = 0.27 ± 0.06 for Fe_3O_4@DMSA–NH_2 NPs), showing a good dispersion in water, which makes them a potent vehicle for drug delivery.

The lattice structure of the as-prepared magnetic nanoparticles were studied by XRD. Fig. 5B shows the XRD patterns of the native Fe_3O_4 nanoparticles. The crystalline diffraction peaks appearing at 30.1°, 35.5°, 43.1°, 57.0° and 62.6° were attributed to the (220), (311), (400), (511) and (440) planes of the spinel phase of Fe_3O_4 (JCPDS No. 65-3107),[38] respectively. The average particle size estimated using Debye–Scherrer's equation was nearly consistent with the results observed in the TEM images, indicating a single crystal of each individual Fe_3O_4 nanoparticle. In addition, the calculated lattice parameter of the nanoparticles from the position of the (311) peak was 8.387 Å, which is quite close to the standard parameter of magnetite (8.396 Å) and relatively far from that of maghemite (8.346 Å), indicating the as-prepared iron oxide nanoparticles are in the magnetite phase.[15] Obviously, there was little difference between the calculated lattice parameters and the standard one, which was probably attributed to the small size induced surface instability of the oxygen stoichiometry of the materials.[15,39,40]

The surface groups of the different functionalized nanoparticles were characterized using FTIR spectroscopy throughout the range of 400–4000 cm^{-1} (Fig. 5C). Fig. 5C(b) shows the FTIR spectrum of the Fe_3O_4@Oley NPs. Compared with the spectrum of oleylamine [Fig. 5C(a)], the methyl stretching bands at ~2930 and 2846 cm^{-1} were because of the oleylamine covering on the surface of the Fe_3O_4 NPs. In Fig. 5C(b), it also exhibits an intense band at ~3510 cm^{-1}, which could be assigned to the stretching vibration of the amino group dating back to the oleylamine molecules. Also a new broad signal at ~580 cm^{-1} was clearly observed,

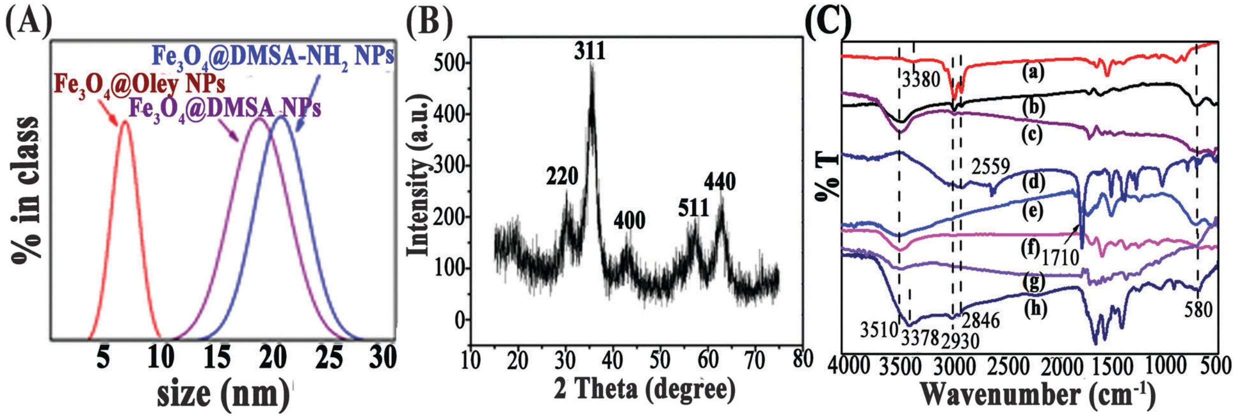

Fig. 5 (A) Dynamic light scattering (DLS) of Fe_3O_4@Oley NPs, Fe_3O_4@DMSA NPs and Fe_3O_4@DMSA–NH_2 NPs; (B) XRD pattern of as-prepared Fe_3O_4@Oley NPs; (C) FT-IR spectrum of (a) oleylamine, (b) Fe_3O_4@Oley NPs, (c) CUR loaded Fe_3O_4@Oley NPs, (d) DMSA, (e) Fe_3O_4@DMSA NPs, (f) CUR loaded Fe_3O_4@DMSA NPs, (g) Fe_3O_4@DMSA–NH_2 NPs, (h) CUR loaded Fe_3O_4@DMSA–NH_2 NPs.

Published on 04 February 2016. Downloaded by CHINA PHARMACEUTICAL UNIVERSITY LIBRARY on 20/12/2016 09:52:56.

which was a characteristic peak of the Fe–O stretching mode in magnetite, indicating the formation of Fe_3O_4@Oley NPs. Fig. 5C(c) shows the FTIR spectrum of the Fe_3O_4@Oley NPs loaded with CUR. Except the characteristic Fe–O absorbance peak at ~589 cm^{-1}, the band appearing at ~3510 cm^{-1} is due to the bending vibration of the phenolic hydroxyl groups in the structure of CUR. In addition, peaks at 2930 and 2846 cm^{-1} are for methoxyl stretching. The FTIR spectrum of the Fe_3O_4@DMSA NPs is shown in Fig. 5C(e). Three characteristic stretching bands are observed at ~550 cm^{-1}, 1230 cm^{-1} and (~1578 and 1650 cm^{-1}) corresponding to the S–S, C–O and C═O stretching of DMSA molecules whose typical IR spectrum is shown in Fig. 5C(d). Although the S–S stretching peak is overlapped by the Fe–O stretching peak at ~580 cm^{-1}, the slight shift to the low wavenumber region and the increased peak intensity at ~550 cm^{-1} verify the formation of S–S crosslinking between the DMSA molecules on the surface of the Fe_3O_4 NPs.[41,42] Fig. 5C(f) shows the FTIR spectrum of the Fe_3O_4@DMSA NPs loaded with CUR. The characteristic bands at ~3510 cm^{-1}, ~1670 cm^{-1}, (1600 and 1500 cm^{-1}), ~1230 cm^{-1} that correspond to the vibration of the hydroxyl groups, carbonyl group, aromatic carbon backbone and phenolic hydroxyl groups in the CUR molecule indicate the loading of CUR on the surface of the Fe_3O_4@DMSA NPs. Fig. 5C(g) shows the spectrum of the Fe_3O_4@DMSA–NH_2 NPs. The ~580 cm^{-1} band is the Fe–O characteristic band. The peaks at ~3400 cm^{-1} and 1610 cm^{-1} are assigned to the amino group on the surface of the particles which are the indication of the successful amination of the nanoparticles. Just as in Fig. 5C(h), in addition to the inherent characteristic peaks of the Fe_3O_4@DMSA–NH_2 NPs, the new emerging bands reference the structure of CUR, indicating the successful loading of the drug on the surface of the particles. Table 1 shows the elemental analysis results of the Fe_3O_4@Oley, Fe_3O_4@DMSA and Fe_3O_4@DMSA–NH_2 NPs. The lines in the table represent that the content of N and S atoms is lower than the detection limit and could not be detected. From the elemental analysis of the Fe_3O_4@DMSA NPs, the absence of nitrogen atoms and the new emergence of S verified the fact that the oleylamine molecules on the surface of the initial Fe_3O_4@Oley NPs were successfully replaced with DMSA. The new emerging N, combined with the increase of C calculated from the potency of N and related molecular weight, indicated the successful amination on the surface of the Fe_3O_4@DMSA–NH_2 NPs. Consistent with the results of FTIR, elemental analysis confirms the construction of the two types of functionalized nanoparticles.

The magnetic properties of the Fe_3O_4@Oley, Fe_3O_4@DMSA and Fe_3O_4@DMSA–NH_2 NPs are shown in Fig. 6A. On the left are the VSM results obtained with an applied magnetic field sweeping from −9 kOe to 9 kOe at room temperature. The magnetic hysteresis loops of the three nanoparticles were S-like and the magnetic remanence was nearly zero. The fact that there was almost no remaining magnetization when the external magnetic field was removed indicated the superparamagnetic properties of the composites at room temperature.[43,44] The magnetic saturation (M_s) values of the Fe_3O_4@DMSA, Fe_3O_4@DMSA–NH_2 and Fe_3O_4@Oley NPs are 29.59, 28.79 and 25.78 emu g^{-1}, respectively. The values of the saturation magnetization for the Fe_3O_4@DMSA and Fe_3O_4@DMSA–NH_2 NPs are nearly same indicating the amination exerting little influence on the magnetism of the functionalized Fe_3O_4 NPs. But the M_s values are slightly higher than that of the original Fe_3O_4@Oley NPs. These phenomena can be attributed to not only the decrease of the nonmagnetic material in Fe_3O_4 formation with high-molecular-weight oleylamine molecules replaced by lower-molecular-weight DMSA, but also the bigger particle size generated due to the aggregation of magnetic nanoparticles during the ligand exchange reaction. This is consistent with the results reported that the M_s values of magnetic nanoparticles vary with their diameters and larger nanoparticles exhibit higher M_s.[43,45] On the right of Fig. 6A are the photographs of the magnetic separation of (a) Fe_3O_4@Oley NPs, (b) Fe_3O_4@DMSA NPs and (c) Fe_3O_4@DMSA–NH_2 NPs dispersed in ethanol. It was observed that the suspensions of the Fe_3O_4@DMSA NPs and Fe_3O_4@DMSA–NH_2 NPs became clear within 40 s when placing a permanent magnet outside the bottle while the Fe_3O_4@Oley NPs dispersion became clear until 75 s, suggesting that the two different types of functionalized Fe_3O_4 NPs have higher magnetism than the Fe_3O_4@Oley NPs, which agrees well with the VSM results.

Due to oleylamine covering the particles, the Fe_3O_4@Oley NPs show properties of hydrophobicity and tend to disperse in nonpolar solvents such as hexane, toluene and chloroform.[15] The two types of functionalized Fe_3O_4 NPs obtained from a ligand exchange reaction and a subsequent amidation reaction tend to be hydrophilic due to the functional groups on the surface of the particles. Fig. 6B shows the photos of the solubility test for the Fe_3O_4@Oley, Fe_3O_4@DMSA and Fe_3O_4@DMSA–NH_2 NPs. The results show that the Fe_3O_4 NPs have been transformed from the organic phase to polar solvents after functionalization and show hydrophilic properties, which is of great significance for the design of drug delivery systems for hydrophobic drugs.

The zeta potential measurement of the two different types of functionalized Fe_3O_4 NPs as a function of pH was carried out to test the surface charge properties. Fig. 6C demonstrates the zeta potential of the Fe_3O_4@DMSA NPs and Fe_3O_4@DMSA–NH_2 NPs measured in the pH range 1–12. The movement of the zeta potential values on the surface of the Fe_3O_4@DMSA–NH_2 NPs towards positive values verifies the successful amination of the Fe_3O_4@DMSA NPs. It can also be observed from the graph that the Fe_3O_4@DMSA–NH_2 NPs have an isoelectric point at approximately 6.23, compared to 2.57 for the Fe_3O_4@DMSA NPs. It is worth noting that when the pH is between 2.57 and 6.23, the surface charge of the Fe_3O_4@DMSA NPs is negative while the Fe_3O_4@DMSA–NH_2 NPs possess a positive charge, which indicates the possibility of increasing the loading capacity of drug

Table 1 Elemental analysis of Fe_3O_4@Oley NPs, Fe_3O_4@DMSA NPs and Fe_3O_4@DMSA–NH_2 NPs

Sample	C (%)	H (%)	N (%)	S (%)
Fe_3O_4@Oley NPs	5.81	1.53	0.34	—
Fe_3O_4@DMSA NPs	5.79	1.31	—	6.63
Fe_3O_4@DMSA–NH_2 NPs	4.63	1.29	0.76	5.27

This journal is © The Royal Society of Chemistry and the Centre National de la Recherche Scientifique 2016

Published on 04 February 2016. Downloaded by CHINA PHARMACEUTICAL UNIVERSITY LIBRARY on 20/12/2016 09:52:56.

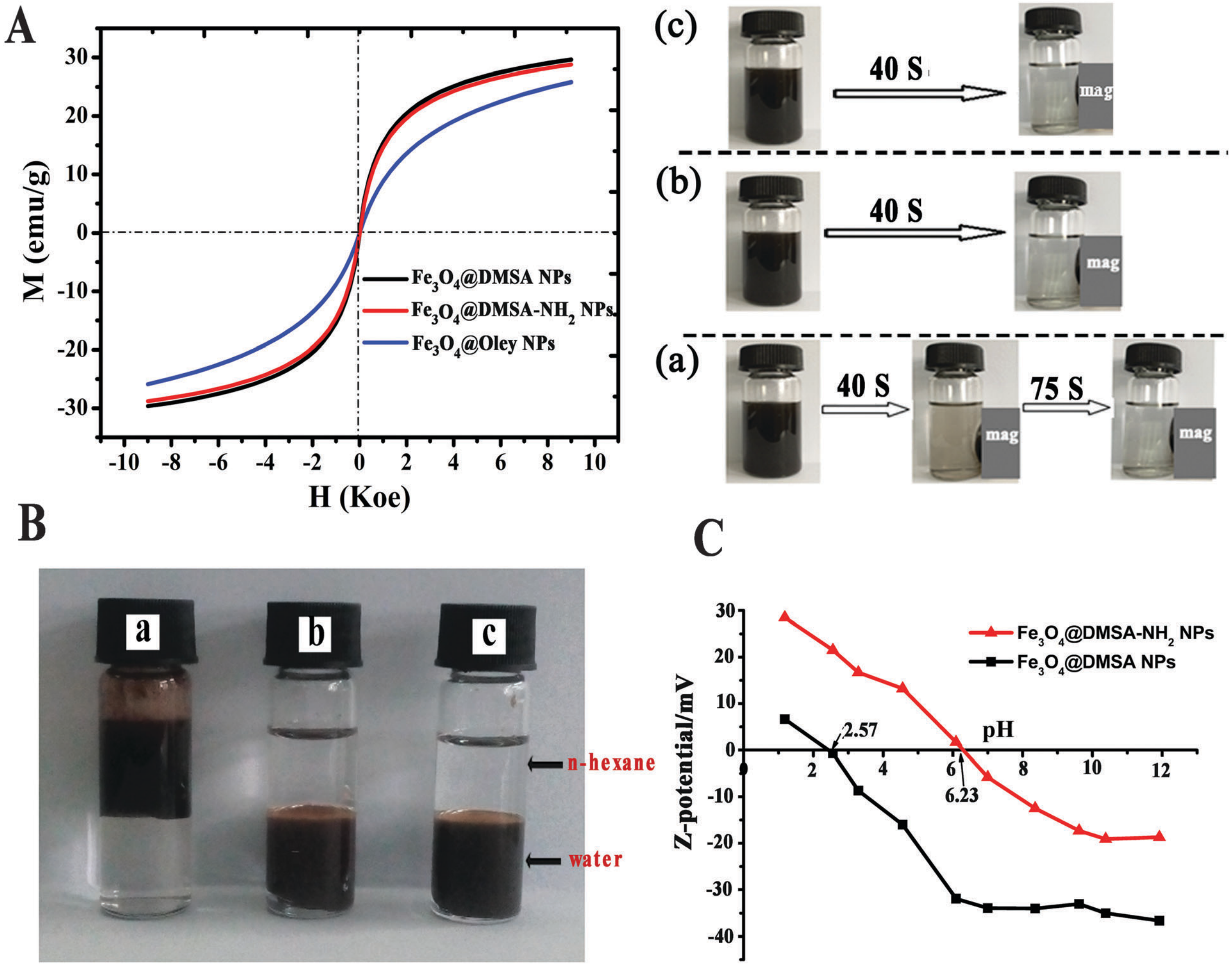

Fig. 6 (A) The VSM results of Fe_3O_4@Oley, Fe_3O_4@DMSA and Fe_3O_4@DMSA–NH_2 NPs and photographs of the magnetic separation of (a) Fe_3O_4@Oley NPs, (b) Fe_3O_4@DMSA NPs and (c) Fe_3O_4@DMSA–NH_2 NPs dispersed in ethanol; (B) photos of the solubility test for (a) Fe_3O_4@Oley, (b) Fe_3O_4@DMSA, (c) Fe_3O_4@DMSA–NH_2 NPs; (C) zeta potential curves of Fe_3O_4@DMSA NPs and Fe_3O_4@DMSA–NH_2 NPs in the pH range 1–12.

carriers for drugs carrying negatively charged groups.[46] Exceptionally, the physical stability of a particle solution can be estimated with the zeta potential of the formulation. After CUR molecules were loaded, the zeta potentials of the Fe_3O_4@DMSA and Fe_3O_4@DMSA–NH_2 NP formulations were respectively −7.36 mV and −3.23 mV, which allows good stability during storage. Because the zeta potential for the nanoparticles in PBS solution (pH 7.4) is a relatively negative value, the nanoparticles are likely to repel each other, resulting in less aggregation.[47–49] The two different types of –COOH or –NH_2 functionalized particles were loaded with hydrophobic curcumin and the dispersity of the composites in PBS solution was investigated. Both dispersion systems kept stable over a number of weeks.

Kinetics analysis

The adsorption kinetics of CUR on Fe_3O_4@Oley NPs, Fe_3O_4@DMSA NPs and Fe_3O_4@DMSA–NH_2 NPs in 75% ethanol water solution at 25 °C are presented in Fig. 7. A rather fast uptake of CUR happened during the first hour and it only took 30 min to reach equilibrium for the Fe_3O_4@Oley NPs while 55 min for the Fe_3O_4@DMSA–NH_2 NPs. For the Fe_3O_4@DMSA NPs about 3 hours had passed before reaching equilibrium and it showed a much slower adsorption process. The adsorption rates of CUR on the Fe_3O_4@Oley, Fe_3O_4@DMSA and Fe_3O_4@DMSA–NH_2 NPs were rapid at the beginning stage and afterwards a slower stage was observed until the adsorption of CUR reached its equilibrium value.

To design and model the adsorption processes, two different models were adopted to calculate the kinetic parameters and interpret the kinetic processes.[50] The pseudo-first-order rate equation is defined as:

$$\ln(q_e - q_t) = \ln q_e - k_1 t \qquad (2)$$

The pseudo-second-order model is shown as follows:

$$\frac{t}{q_t} = \frac{t}{q_e} + \frac{1}{k_2 q_e} \qquad (3)$$

where q_e and q_t (mg g^{-1}) are the adsorbed amounts of CUR at equilibrium and at time t (min); k_1 and k_2 represent the equilibrium rate constant for the pseudo-first-order model and pseudo-second-order model, respectively. Straight lines from plots of $\ln(q_e - q_t)$ and t/q_t *versus* t were fitted from the kinetic data.

Published on 04 February 2016. Downloaded by CHINA PHARMACEUTICAL UNIVERSITY LIBRARY on 20/12/2016 09:52:56.

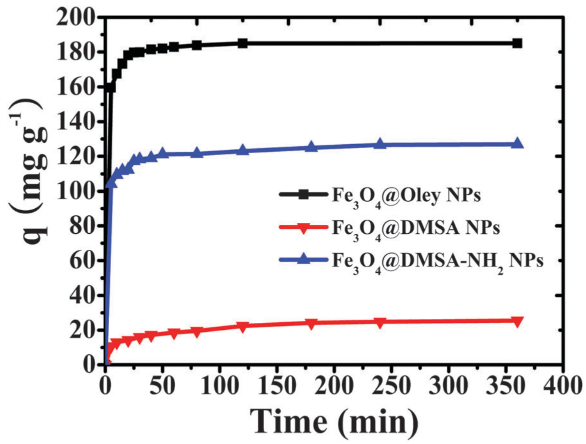

Fig. 7 Kinetic curves for CUR adsorption on different Fe_3O_4 NPs (CUR concentration 200 μg mL^{-1}, adsorbent dose 0.8 mg mL^{-1}, temperature 25 °C, pH 5.4).

The adsorption kinetics processes of the three nanoparticles are found to fit better with the pseudo-second-order model with higher values of correlation coefficient.[51] The rate constants calculated from the fitted plots are listed in Table 2. This result suggests that the adsorption rate of CUR depends on the concentration of CUR at the surface of adsorbents and the amount of drugs adsorbed at equilibrium.

Adsorption isotherms

The adsorption isotherm demonstrates the relationship between adsorption capacity at equilibrium and equilibrium concentration at a specific temperature. Fig. 8 represents the adsorption isotherms of CUR on the Fe_3O_4@Oley, Fe_3O_4@DMSA and Fe_3O_4@DMSA–NH_2 NPs at 25 °C. In general, the equilibrium adsorption capacity increases with the equilibrium concentration until the value of initial concentration reaches a certain point. The Langmuir model and the Freundlich model are widely used modes for the description of the adsorption isotherm. The Langmuir model is used to describe the monolayer adsorption behavior on a homogeneous surface with limited adsorption sites and is expressed as follows:

$$\frac{1}{q_e} = \frac{1}{Q_m} + \frac{1}{Q_m C_e K_L} \tag{4}$$

where Q_m is the maximum adsorption capacity of CUR; q_e represents the equilibrium CUR concentration absorbed on the materials (mg g^{-1}); C_e is the equilibrium concentration of CUR in solution (mg mL^{-1}) and K_L is the Langmuir constant concerning the affinity of the adsorption sites.

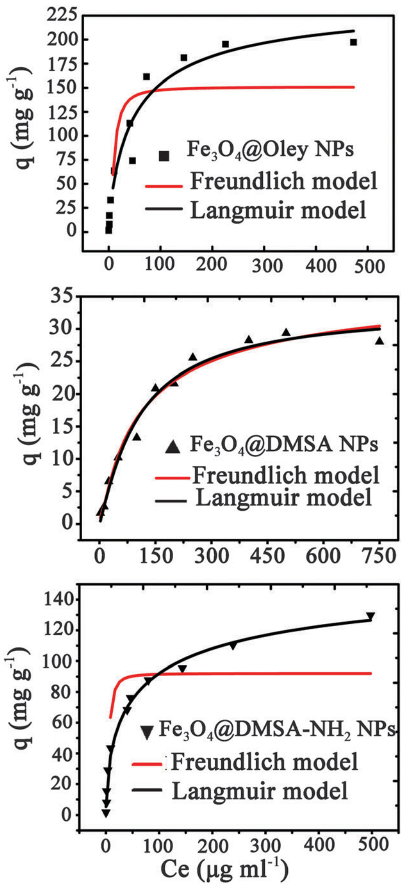

Fig. 8 Adsorption isotherms of CUR on different materials (adsorbent dose 0.8 mg mL^{-1}, temperature 25 °C, pH 5.40, equilibrium time 4 h).

The Freundlich isotherm applies to studying the absorption on heterogeneous surfaces with varied affinity sites and the related sorption energy changing exponentially. The equation is described as:

$$\lg q_e = \lg K_F + \frac{\lg C_e}{n} \tag{5}$$

where q_e is the equilibrium absorbed concentration on the materials (mg g^{-1}); C_e is the equilibrium concentration of CUR in solution (mg mL^{-1}); K_F and n, the Freundlich constants, are related to the adsorption capacity and adsorption intensity, respectively.

The equilibrium adsorption data of CUR on the Fe_3O_4@Oley, Fe_3O_4@DMSA and Fe_3O_4@DMSA–NH_2 NPs was studied by the Langmuir and Freundlich isotherm models (Fig. 8). The adsorbed amount of CUR was found to increase with increasing concentration of CUR at equilibrium. The values of the correlation coefficient

Table 2 Adsorption kinetic constants for CUR adsorption on Fe_3O_4@Oley NPs, Fe_3O_4@DMSA NPs, and Fe_3O_4@DMSA–NH_2 NPs at 25 °C

	Pseudo-first-order kinetic model				Pseudo-second-order kinetic model		
Materials	$q_{e,exp}$ (mg g^{-1})	$q_{e,cal}$ (mg g^{-1})	k_1 (min)	R_1^2	$q_{e,cal}$ (mg g^{-1})	k_2 (g mg^{-1} min^{-1})	R_2^2
Fe_3O_4@Oley NPs	184.96	26.17	0.0482	0.9478	185.19	0.0052	0.9997
Fe_3O_4@DMSA NPs	25.62	15.95	0.0118	0.9838	26.25	0.0023	0.9983
Fe_3O_4@DMSA–NH_2 NPs	126.89	17.58	0.0149	0.9378	128.21	0.0031	0.9999

Published on 04 February 2016. Downloaded by CHINA PHARMACEUTICAL UNIVERSITY LIBRARY on 20/12/2016 09:52:56.

Table 3 Adsorption isotherm constants for CUR adsorption on Fe_3O_4@Oley NPs, Fe_3O_4@DMSA NPs, and Fe_3O_4@DMSA–NH_2 NPs at 25 °C

	Freundlich isotherm model			Langmuir isotherm model		
Materials	K_F	n	R^2	Q_m	K_L	R^2
Fe_3O_4@Oley NPs	9.32	1.68	0.7792	208.33	0.03	0.9535
Fe_3O_4@DMSA NPs	0.96	1.77	0.9791	33.33	0.01	0.9822
Fe_3O_4@DMSA–NH_2 NPs	8.21	1.95	0.8087	129.87	0.03	0.9920

R^2 and the constants calculated from the two models are presented in Table 3.

The results revealed that the Langmuir model better described the CUR adsorption data for the three kinds of Fe_3O_4 nanoparticles with much higher R^2 values, indicating the homogeneous nature of the particle surfaces and thus identical adsorption activation energy for each CUR molecule. The maximum amounts of CUR adsorbed to the Fe_3O_4@Oley, Fe_3O_4@DMSA and Fe_3O_4@DMSA–NH_2 NPs were calculated to be 208.33, 33.33 and 129.87 mg g^{-1}, respectively.

Drug loading mechanism

In summary, the data and constants from the adsorption experiments including kinetics analysis and adsorption isotherms demonstrated the order of adsorption affinity which was as follows: Fe_3O_4@Oley NPs > Fe_3O_4@DMSA–NH_2 NPs > Fe_3O_4@DMSA NPs. This can be illuminated by the mechanisms of CUR loading on the three kinds of nanoparticles. For Fe_3O_4@Oley NPs, the loading of CUR was due to the strong hydrophobic interactions under the conditions of the polar solvent and therefore a much higher adsorption capacity (with 184.96 μg CUR per one mg of nanoparticles) was achieved. When the oleylamine molecules on the surface of Fe_3O_4@Oley NPs were replaced by DMSA, because of the lack of enough groups fabricating hydrogen bonds, Fe_3O_4@DMSA presented limited drug loading. After the amination reaction, Fe_3O_4@DMSA–NH_2 NPs showed an improved loading capacity for CUR, which could be attributed to the cooperating results of not only the hydrogen bonds, but also the enhanced hydrophobic interactions under the relatively polar conditions due to prolonged chain generated through the amidation reaction. Although CUR has shown great potential as an anti-tumor agent, its widespread use in tumor treatment is hindered by its poor aqueous solubility and low bioavailability. In past decades, extensive efforts have been devoted to developing novel formulations for CUR to solve this issue. All together, the Fe_3O_4@DMSA–NH_2 NPs possessed advantages over both the Fe_3O_4@Oley and Fe_3O_4@DMSA NPs, such as hydrophilicity and high adsorption capacity and they have remarkable potency to be developed as MTDDS for hydrophobic drugs like CUR.

In vitro drug release

The amount of CUR loaded onto particles was quantified using a UV-Vis spectrophotometer. The loading of CUR was 95.57% (139.86 μg mg^{-1}), 18.37% (23.55 μg mg^{-1}) and 76.29% (111.64 μg mg^{-1}) respectively for the Fe_3O_4@Oley, Fe_3O_4@DMSA and Fe_3O_4@DMSA–NH_2 NPs. The release experiments *in vitro* were carried out at 37 °C, the temperature of human body. The *in vitro* release profiles of CUR from the three formulations of nanoparticles in PBS solution at different pH values are shown as Fig. 9. The blue lines in each plot represent the equilibrium point of drug release. From the figures, it could be indicated that the adsorption of CUR on the particles was reversible and showed a rapid release process in the early stage, followed by a slow and sustained release stage, which is consistent with the previous report that the desorption of chemical substances from sediment often occurs in two stages: a quick release of a labile adsorbed fraction, then a slow release of a steady fraction.[52]

The solubility of drug in the release medium plays an important role in the desorption profiles of the drug from the delivery system. As shown in Fig. 9, the amounts of CUR released from the Fe_3O_4@Oley, Fe_3O_4@DMSA and Fe_3O_4@DMSA–NH_2 NPs in neutral solution are respectively about 52%, 73% and 76%, while 50%, 62% and 60% in acidic solution. Compared with related literature,[11,53] the cumulative release rates from the two types of functionalized nanoparticles under neutral conditions were slightly lower, while the hydrophobic Fe_3O_4@Oley NPs show a relatively low release rate, which may be interpreted by not only the strong hydrophobic interaction, but also the poor solubility

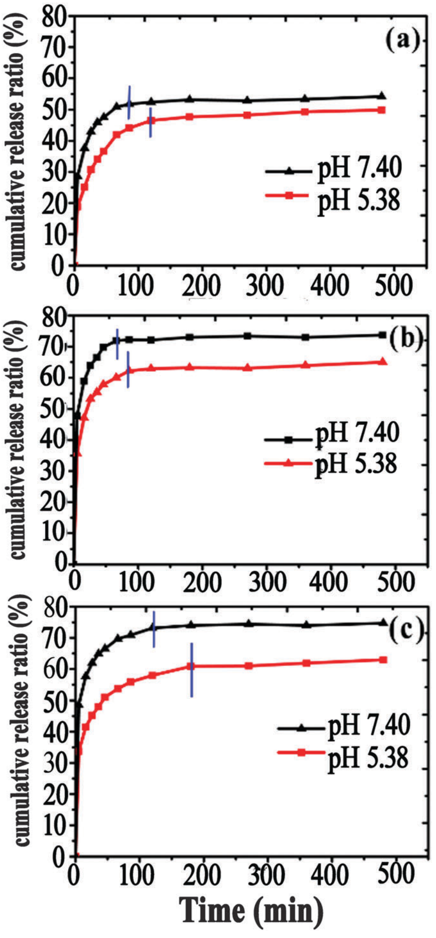

Fig. 9 Cumulative release results of CUR from (a) Fe_3O_4@Oley, (b) Fe_3O_4@DMSA and (c) Fe_3O_4@DMSA–NH_2 NPs at different pH at 37 °C.

Published on 04 February 2016. Downloaded by CHINA PHARMACEUTICAL UNIVERSITY LIBRARY on 20/12/2016 09:52:56.

Table 4 Release of CUR from different materials at different pH

	Release percentage (%) ($n = 6$)			
Materials	pH 5.38	RSD (%)	pH 7.40	RSD (%)
Fe_3O_4@Oley NPs	49.89	2.31	54.21	2.56
Fe_3O_4@DMSA NPs	64.98	2.56	74.53	1.98
Fe_3O_4@DMSA–NH_2 NPs	58.39	3.01	73.68	2.61

of CUR in the polar PBS solution. Furthermore, as shown in Table 4, the cumulative release rates of CUR from all the three nanoparticles, shaken for 8 h, in the acidic medium (pH 5.38) was lower than that in the physiological pH medium (pH 7.40). This phenomenon could be due to the keto–enol tautomerization of CUR and the enol form is the preferential conformation under acidic conditions, which will fabricate much stronger hydrogen bonds and hydrophobic interactions and thus lower solubility in the release medium. Interestingly, compared with the two other types of particles, the Fe_3O_4@DMSA–NH_2 NPs show a prolonged and even slightly longer release time at pH 5.38, which is because of hydrogen bonds under acidic conditions and enhanced hydrophobic actions under polar conditions due to the prolonged chains generated through the amidation reaction. It has been reported that the local pH of tumor cells ($pH < 6.5$) is lower than that of normal cells (pH 7.40).[54,55] Therefore, the pH-sensitive release behavior of CUR from Fe_3O_4@DMSA–NH_2 NPs may benefit the tumor treatment.

Conclusion

In summary, superparamagnetic Fe_3O_4 nanoparticles with chemical stability, small size, narrow size distribution and good magnetic properties were fabricated using a very simplified method based on the solvothermal decomposition of $Fe(acac)_3$ in a high-boiling organic solvent with oleylamine as both the reducing agent and stabilizer. The resulting oleylamine-coated nanoparticles (~4.3 nm in diameter) were carboxylated by *meso*-2,3-dimercaptosuccinic acid (DMSA) ligand-exchange reactions and subsequently aminated to obtain carboxyl-functionalized and amino-functionalized Fe_3O_4 nanoparticles. The two types of functionalized magnetic nanoparticles were characterized and designed as drug carriers to load a natural antitumor drug, curcumin. The loading processes could be described by the Langmuir adsorption isothermal model for both functionalized Fe_3O_4 NPs and the pseudo-second-order model fitted well with the kinetic data. In addition, the drug release of all particles showed to be pH-sensitive. On comprehensive consideration, the Fe_3O_4 nanoparticles carrying the –NH_2 group (Fe_3O_4@DMSA–NH_2 NPs) have advantages over the initial nanoparticles (Fe_3O_4@Oley NPs) and carboxylated nanoparticles (Fe_3O_4@DMSA NPs) such as high loading capacity, hydrophilicity, and a prolonged drug release. Due to these properties, the functionalized nanoparticles have great promise to be utilized in engineered magnetic targeted drug delivery systems for curcumin to improve its water solubility and bioavailability. This study will enrich the theoretical research on functionalization in the design of drug delivery systems for hydrophobic drugs.

Acknowledgements

This study was supported by the National Natural Science Foundation of China (Grant No. 81402899), the Open Project of the Key Laboratory of Modern Toxicology of the Ministry of Education (Grant No. NMUMT201404), the Jiangsu Province Science Foundation for Youths (BK20130644), the National Basic Science Personal Training Fund (No. J0630858) and the College Students Innovation Project for the R&D of Novel Drugs and the National Found for Fostering Talents of Basic Science (NFFTBS)-Provincial Innovation and Entrepreneurship Training Program for College Students (No. J1030830). The authors also gratefully acknowledge trainees Yating Zheng and Ningning Lin who participated in the data collecting and discussions with colleagues in the research group.

Notes and references

1 J. Safari and Z. Zarnegar, *J. Saudi Chem. Soc.*, 2014, **18**, 85–99.
2 L. Guo, W. Ding and L.-M. Zheng, *J. Nanosci. Nanotechnol.*, 2014, **14**, 4858–4864.
3 Y. Wang, R. Huang, G. Liang, Z. Zhang, P. Zhang, S. Yu and J. Kong, *Small*, 2014, **10**, 109–116.
4 Y.-X. J. Wang, S. Xuan, M. Port and J.-M. Idee, *Curr. Pharm. Des.*, 2013, **19**, 6575–6593.
5 S. Laurent, A. A. Saei, S. Behzadi, A. Panahifar and M. Mahmoudi, *Expert Opin. Drug Delivery*, 2014, **11**, 1449–1470.
6 B. Issa, I. M. Obaidat, B. A. Albiss and Y. Haik, *Int. J. Mol. Sci.*, 2013, **14**, 21266–21305.
7 J. A. Kim, J.-H. Choi, M. Kim, W. J. Rhee, B. Son, H.-K. Jung and T. H. Park, *Biomaterials*, 2013, **34**, 8555–8563.
8 F. Ye, A. Barrefelt, H. Asem, M. Abedi-Valugerdi, I. El-Serafi, M. Saghafian, K. Abu-Salah, S. Alrokayan, M. Muhammed and M. Hassan, *Biomaterials*, 2014, **35**, 3885–3894.
9 L. Ao, B. Wang, P. Liu, L. Huang, C. Yue, D. Gao, C. Wu and W. Su, *Nanoscale*, 2014, **6**, 10710–10716.
10 J. Li, Y. He, W. Sun, Y. Luo, H. Cai, Y. Pan, M. Shen, J. Xia and X. Shi, *Biomaterials*, 2014, **35**, 3666–3677.
11 S. Manju, C. P. Sharma and K. Sreenivasan, *J. Mater. Chem.*, 2011, **21**, 15708.
12 S. Meerod, B. Rutnakornpituk, U. Wichai and M. Rutnakornpituk, *J. Magn. Magn. Mater.*, 2015, **392**, 83–90.
13 J. Salado, M. Insausti, L. Lezama, I. Gil de Muro, E. Goikolea and T. f. Rojo, *Chem. Mater.*, 2011, **23**, 2879–2885.
14 A. G. Roca, S. Veintemillas-Verdaguer, M. Port, C. Robic, C. J. Serna and M. P. Morales, *J. Phys. Chem. B*, 2009, **113**, 7033–7039.
15 Z. C. Xu, C. M. Shen, Y. L. Hou, H. J. Gao and S. S. Sun, *Chem. Mater.*, 2009, **21**, 1778–1780.
16 M. Heidari Majd, D. Asgari, J. Barar, H. Valizadeh, V. Kafil, A. Abadpour, E. Moumivand, J. S. Mojarrad, M. R. Rashidi, G. Coukos and Y. Omidi, *Colloids Surf., B*, 2013, **106**, 117–125.
17 S. Sundar, R. Mariappan and S. Piraman, *Powder Technol.*, 2014, **266**, 321–328.

This journal is © The Royal Society of Chemistry and the Centre National de la Recherche Scientifique 2016

Published on 04 February 2016. Downloaded by CHINA PHARMACEUTICAL UNIVERSITY LIBRARY on 20/12/2016 09:52:56.

18 N. Dayyani, S. Khoee and A. Ramazani, *Eur. J. Med. Chem.*, 2015, **98**, 190–202.

19 A. Pourjavadi, S. H. Hosseini, M. Alizadeh and C. Bennett, *Colloids Surf., B*, 2014, **116**, 49–54.

20 M. Y. Hua, H. W. Yang, C. K. Chuang, R. Y. Tsai, W. J. Chen, K. L. Chuang, Y. H. Chang, H. C. Chuang and S. T. Pang, *Biomaterials*, 2010, **31**, 7355–7363.

21 S. Yang, D. Chen, N. Li, X. Mei, X. Qi, H. Li, Q. Xu and J. Lu, *J. Mater. Chem.*, 2012, **22**, 25354–25361.

22 M. M. Yallapu, M. C. Ebeling, S. Khan, V. Sundram, N. Chauhan, B. K. Gupta, S. E. Puumala, M. Jaggi and S. C. Chauhan, *Mol. Cancer Ther.*, 2013, **12**, 1471–1480.

23 H. Ligeret, S. Barthelemy, R. Zini, J.-P. Tillement, S. Labidalle and D. Morin, *Free Radicals Biol. Med.*, 2004, **36**, 919–929.

24 D. Stefanakis and D. Ghanotakis, *J. Nanopart. Res.*, 2013, **16**, 2211.

25 Y. Hou, Z. Xu and S. Sun, *Angew. Chem., Int. Ed.*, 2007, **46**, 6329–6332.

26 M. Gogoi, P. Deb, G. Vasan, P. Keil, A. Kostka and A. Erbe, *Appl. Surf. Sci.*, 2012, **258**, 9685–9691.

27 M. Menelaou, K. Georgoula, K. Simeonidis and C. Dendrinou-Samara, *Dalton Trans.*, 2014, **43**, 3626–3636.

28 P. B. H. HU, B. Zhao, M. A. Hamon, M. E. Itkis and R. C. Haddon, *Chem. Phys. Lett.*, 2001, **345**, 4.

29 H. P. Boehm, *Carbon*, 2002, **40**, 145–149.

30 R. N. Mitra, M. Doshi, X. Zhang, J. C. Tyus, N. Bengtsson, S. Fletcher, B. D. G. Page, J. Turkson, A. J. Gesquiere, P. T. Gunning, G. A. Walter and S. Santra, *Biomaterials*, 2012, **33**, 1500–1508.

31 M.-H. Pan, Y.-J. Wang, A.-L. Cheng, L.-I. Lin, Y.-S. Ho, C.-Y. Hsieh and J.-K. Lin, *J. Pharm. Biomed. Anal.*, 1996, **15**(1997), 1867–1876.

32 C. Cannas, A. Musinu, A. Ardu, F. Orru, D. Peddis, M. Casu, R. Sanna, F. Angius, G. Diaz and G. Piccaluga, *Chem. Mater.*, 2010, **22**, 3353–3361.

33 S. Carenco, C. D. Boissière, L. Nicole, C. M. Sanchez, P. Le Floch and N. Mézailles, *Chem. Mater.*, 2010, **22**, 1340–1349.

34 S. H. Sun and H. Zeng, *J. Am. Chem. Soc.*, 2002, **124**, 8204–8205.

35 T. Yang, C. Shen, Z. Li, H. Zhang, C. Xiao, S. Chen, Z. Xu, D. Shi, J. Li and H. Gao, *J. Phys. Chem. B*, 2005, **109**, 23233–23236.

36 T. Jani, J. H. J. Ann-Cathrin, H. Jenny Perez, G. Stefan, A. G.-U. Julián, O. Eva, B. C. P. Jan and H. Martin, *Sci. Technol. Adv. Mater.*, 2014, **15**, 035009.

37 T. Eslaminejad, S. N. Nematollahi-Mahani and M. Ansari, *J. Magn. Magn. Mater.*, 2016, **402**, 34–43.

38 S. Li, Y. Gong, Y. Yang, C. He, L. Hu, L. Zhu, L. Sun and D. Shu, *Chem. Eng. J.*, 2015, **260**, 231–239.

39 N. Guigue-Millot, S. Begin-Colin, Y. Champion, M. J. Hytch, G. Le Caer and P. Perriat, *J. Solid State Chem.*, 2003, **170**, 30–38.

40 T. J. Daou, G. Pourroy, S. Begin-Colin, J. M. Greneche, C. Ulhaq-Bouillet, P. Legare, P. Bernhardt, C. Leuvrey and G. Rogez, *Chem. Mater.*, 2006, **18**, 4399–4404.

41 L. I. Cabrera, Á. Somoza, J. F. Marco, C. J. Serna and M. Puerto Morales, *J. Nanopart. Res.*, 2012, **14**, 873.

42 Y. M. Huh, Y. W. Jun, H. T. Song, S. Kim, J. S. Choi, J. H. Lee, S. Yoon, K. S. Kim, J. S. Shin, J. S. Suh and J. Cheon, *J. Am. Chem. Soc.*, 2005, **127**, 12387–12391.

43 P. Liu, W. Zhong, X. Wu and J. Qiu, *Chem. Eng. J.*, 2013, **219**, 10–18.

44 S. Patra, E. Roy, P. Karfa, S. Kumar, R. Madhuri and P. K. Sharma, *ACS Appl. Mater. Interfaces*, 2015, **7**, 9235–9246.

45 Y. Chen, Y. Wang, H.-B. Zhang, X. Li, C.-X. Gui and Z.-Z. Yu, *Carbon*, 2015, **82**, 67–76.

46 S. Del Buffa, E. Grifoni, F. Ridi and P. Baglioni, *J. Nanopart. Res.*, 2015, **17**, 146.

47 S. Chauhan, M. Yallapu, S. Othman, E. Curtis, N. Bauer, N. Chauhan, M. Jaggi and D. Kumar, *Int. J. Nanomed.*, 2012, **7**, 1761–1779.

48 N. Han, Y. Wang, J. Bai, J. Liu, Y. Wang, Y. Gao, T. Jiang, W. Kang and S. Wang, *Microporous Mesoporous Mater.*, 2016, **219**, 209–218.

49 M. V. Barbosa, L. O. F. Monteiro, G. Carneiro, A. R. Malagutti, J. M. C. Vilela, M. S. Andrade, M. C. Oliveira, A. D. Carvalho-Junior and E. A. Leite, *Colloids Surf., B*, 2015, **136**, 553–561.

50 S. Mane, S. Ponrathnam and N. Chavan, *New J. Chem.*, 2015, **39**, 3835–3844.

51 P. Dramou, P. Zuo, H. He, L. A. Pham-Huy, W. Zou, D. Xiao, C. Pham-Huy and T. Ndorbor, *J. Mater. Chem. B*, 2013, **1**, 4099.

52 B. Sundelin, A.-K. Eriksson Wiklund, G. Lithner and Ö. Gustafsson, *Environ. Toxicol. Chem.*, 2004, **23**, 2611.

53 K. Delmar and H. Bianco-Peled, *Carbohydr. Polym.*, 2016, **136**, 570–580.

54 X. Zhang, L. Meng, Q. Lu, Z. Fei and P. J. Dyson, *Biomaterials*, 2009, **30**, 6041–6047.

55 Y. Dong, Z. Zhou, H. Ding and S. Zhang, *Pharm. Dev. Technol.*, 2014, **19**, 960–967.